arXiv:1512.05561v1 [cond-mat.mes-hall] 17 Dec 2015

Coherence from vacuum fluctuations

Pasi Lähteenmäki[1], G. S. Paraoanu[1], Juha Hassel[2], & Pertti. J. Hakonen[1]

[1]*Low Temperature Laboratory, Department of Applied Physics, Aalto University School of Science, P.O. Box 15100, FI-00076 AALTO, Finland*

[2]*VTT Technical Research Centre of Finland, 02044, Espoo, Finland*

December 18, 2015

The existence of vacuum fluctuations is one of the most important predictions of modern quantum field theory. In the vacuum state, fluctuations occurring at different frequencies are uncorrelated. However, if a parameter in the Lagrangian of the field is modulated by an external pump, vacuum fluctuations stimulate spontaneous downconversion processes, creating squeezing between modes symmetric with respect to half of the frequency of the pump. Here we show that by double parametric pumping of a superconducting microwave cavity in the ground state, it is possible to generate another fundamental type of correlation, namely coherence between photons in separate frequency modes that are not directly connected through a single downconversion process. The coherence is tunable by the phases of the pumps and it is established by a quantum fluctuation that takes simultaneously part in creation of two photon pairs. Our analysis indicates that the origin of this vacuum-induced coherence is the absence of "which-way" information in the frequency space.

A fundamental result in quantum field theory is that fluctuations of the quantum vacuum

at different frequencies are uncorrelated. In parametrically modulated superconducting circuits [1–3], it has been demonstrated that vacuum fluctuations trigger the creation of two-mode squeezed microwave photons [4–12], a key element in all quantum computational models with continuous variables [13]. Furthermore, recent experimental investigations of such effects in superconducting microwave circuits have been interpreted to provide beautiful analogies with the motion of a mirror in free space [8,9], also referred to as dynamical Casimir effect. However, for realizing the envisioned potential of this effect for quantum computing with continuous variables in microwave circuits [14] much more complex quantum states would be needed. Here we demonstrate that tripartite quantum states displaying both coherence and squeezing correlations can be created from vacuum fluctuations by employing another fundamental quantum-mechanical principle, that of absence of which-way information [15,16], applied here in the frequency space. Specifically, we study the parametric modulation of the quantum vacuum under the action of two pumps. We demonstrate that a non-zero coherent correlation $\langle \tilde{a}_1^\dagger \tilde{a}_2 \rangle$ is established between two frequency modes $\tilde{a}_1$ and $\tilde{a}_2$, through downconversion processes in the two pumps triggered by the same vacuum fluctuation in a third frequency mode $\tilde{a}_0$. This correlation is non-zero provided that it is not possible to specify from which pump the photons at $\tilde{a}_0$ originate from. Due to this coherence effect a highly-populated "bright" mode and, orthogonal to it, a zero-population "dark" mode can be defined in the subspace of the two frequency modes. Dark states appear as a result of destructive quantum interference. Typically, in atomic physics, optics, and more recently in superconducting microwave systems, this is realized in Rabi-driven multilevel quantum systems [17], or, in the case of resonators, by sideband driving [18,19], both of which use Hamiltonians of the type $a^\dagger b + h.c.$ to simply transfer population

from one level to another. In contrast, here our Hamiltonian is of parametric type $a^\dagger a^\dagger + h.c.$ which creates populations from the vacuum instead of transferring them between levels. These parametric coherence effects are phase-sensitive phenomena and they can be controlled by the relative phase of the applied pumps.

Our system consists of a superconducting resonator (see Fig. 1) which can be described by the effective Hamiltonian [9]

$$H = \hbar\omega_{\rm res} a^\dagger a + \frac{\hbar}{2i}\sum_{p=1,2}\left[\alpha_p^* e^{i\omega_p t+\varphi_p} - \alpha_p e^{-i\omega_p t-\varphi_p}\right](a+a^\dagger)^2, \tag{1}$$

where α_p is the strength of pump p coupled into the resonator, in units of frequency, and φ_p specifies the pump phase. Denoting the decay rate of the resonator by κ and setting $\xi = \omega - \omega_{\rm res}$, the output field $\tilde{a}_{\rm out}[\xi] = \tilde{a}_{\rm in}[\xi] + \sqrt{\kappa}\tilde{a}[\xi]$ is obtained within the input-output formalism by solving iteratively the Heisenberg-Langevin equations in a rotating frame at the resonator frequency defined by $\tilde{a}(t) = e^{i\omega_{\rm res}t}a(t)$. We obtain a nested structure

$$\tilde{a}_{\rm out}[\xi] = \left[1 - \frac{\kappa\chi(\xi)}{1-\sum_{p=1}^2 \mathcal{N}_1^{[p]}(\xi)}\right] a_{\rm in}[\xi] - \\ -\frac{\kappa\chi(\xi)}{1-\sum_{p=1}^2 \mathcal{N}_1^{[p]}(\xi)}\sum_{p=1}^{2}\frac{\alpha_p\chi^*(2\Delta_p-\xi)}{\mathcal{N}_2^{[p]}(\xi)}\left[(\tilde{a}_{\rm in}[2\Delta_p-\xi])^\dagger + \frac{\alpha_{\bar{p}}^*\chi(2\Delta_{\bar{p}}-2\Delta_p+\xi)}{\mathcal{N}_3^{[p]}(\xi)}\tilde{a}_{\rm in}[2\Delta_{\bar{p}}-2\Delta_p+\xi]+\dots\right]. \tag{2}$$

Here $\chi(\xi) = (\kappa/2 - i\xi)^{-1}$ is the electrical susceptibility of the resonator, $\bar{p} \in \{1,2\} \setminus \{p\}$, and $\mathcal{N}_j^{[p]}$ denote normalization factors (see the Supplementary information).

For simplification, we truncate Eq. (2) to the first-order reflections of ξ with respect to the pumps, and assume $|\Delta_p| >> |\xi|$. In this approximation $\mathcal{N}_2^{[p]}(\xi) \approx 1$, which together with a pump asymmetry parametrization by an angle θ, $\alpha_1\chi^*(2\Delta_1) = \cos\theta\tanh(\lambda/2)e^{i\varphi_1}$, and $\alpha_2\chi^*(2\Delta_2) =$

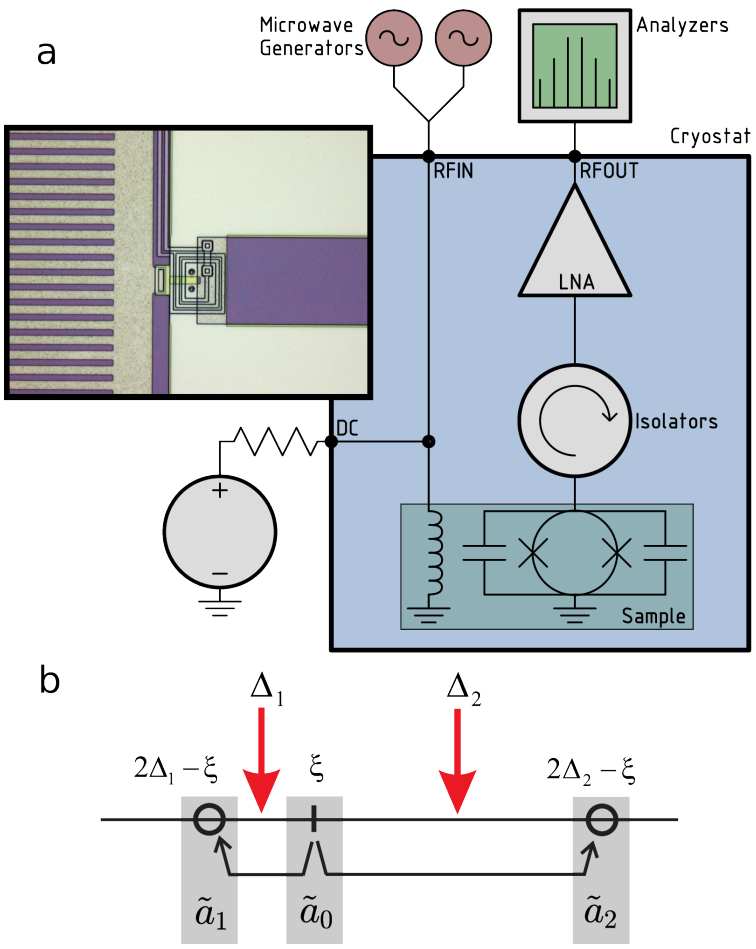

Figure 1: a) Simplified schematic of the measurement setup (see Supplementary information for a more detailed schematic). The investigated resonator was made using a capacitively shunted superconducting quantum interference device (SQUID), fabricated using a NbAlO$_x$Nb trilayer process at VTT[20]. The device forms a flux tunable resonator which acts as a tunable boundary condition for the reflected waves in the 50 Ω transmission line[9]. The designed critical current for the junctions of the SQUID was $I_C = 33$ μA, and the total parallel capacitance was $C = 40$ pF. The experiments were performed at 15 mK, which corresponds to a thermal occupation number of $\overline{n} = 1 \times 10^{-7}$ at the 5 GHz fundamental frequency of the resonator. Modulation of the flux through the SQUID is realized through a lithographically fabricated rectangular spiral coil underneath the junction layer. b) Illustration of the first reflections of a frequency $\xi = \omega - \omega_{\rm res}$ with respect to half the pump frequencies $\Delta_p = \omega_p/2 - \omega_{\rm res}$.

$\sin\theta\tanh(\lambda/2)e^{i\varphi_2}$, allows us to introduce 'bright' and 'dark' modes,

$$\tilde{b}[\xi] = \cos\theta e^{-i\varphi_1}\tilde{a}[2\Delta_1-\xi]+\sin\theta e^{-i\varphi_2}\tilde{a}[2\Delta_2-\xi], \quad (3)$$

$$\tilde{d}[\xi] = \sin\theta e^{-i\varphi_1}\tilde{a}[2\Delta_1-\xi]-\cos\theta e^{-i\varphi_2}\tilde{a}[2\Delta_2-\xi]. \quad (4)$$

These two modes are orthogonal to each other, spanning the Hilbert space of the extremal modes $2\Delta_1-\xi$ and $2\Delta_2-\xi$. The definition of the modes $\tilde{b}$ and $\tilde{d}$ resembles a beam-splitter/merging operation in frequency (rather than in space, as in usual interferometers), where a mode is separated into two branches with a distance $2(\Delta_1-\Delta_2)$ between them. The parameter λ corresponds to the usual two mode squeezing parameter [12].

Having the input state as the vacuum, several types of correlation will be established in the output field. Each pump will produce squeezing correlations $\langle\tilde{a}_{\rm out}[\xi]\tilde{a}_{\rm out}[2\Delta_1-\xi']\rangle = \frac{1}{2}\cos\theta\exp(i\varphi_1)\sinh 2\lambda\times\delta(\xi-\xi')$, $\langle\tilde{a}_{\rm out}[\xi]\tilde{a}_{\rm out}[2\Delta_2-\xi']\rangle = \frac{1}{2}\exp(i\varphi_2)\sin\theta\sinh 2\lambda\times\delta(\xi-\xi')$ as well as noise at $2\Delta_1-\xi$ and $2\Delta_2-\xi$, according to the dynamical Casimir effect power noise formula[9] for each pump separately, $\left\langle(\tilde{a}_{\rm out}[2\Delta_1-\xi])^\dagger\tilde{a}_{\rm out}[2\Delta_1-\xi']\right\rangle = \cos^2\theta\sinh^2\lambda\times\delta(\xi-\xi')$, $\left\langle(\tilde{a}_{\rm out}[2\Delta_2-\xi])^\dagger\tilde{a}_{\rm out}[2\Delta_2-\xi']\right\rangle = \sin^2\theta\sinh^2\lambda\times\delta(\xi-\xi')$, while at ξ the noise is produced by the action of both pumps, $\left\langle(\tilde{a}_{\rm out}[\xi])^\dagger\tilde{a}_{\rm out}[\xi']\right\rangle = \sinh^2\lambda\times\delta(\xi-\xi')$. Surprisingly, the simultaneous action of the two pumps produces the correlation $\left\langle(\tilde{a}_{\rm out}[2\Delta_1-\xi])^\dagger\tilde{a}_{\rm out}[2\Delta_2-\xi']\right\rangle = \left(\left\langle(\tilde{a}_{\rm out}[2\Delta_2-\xi])^\dagger\tilde{a}_{\rm out}[2\Delta_1-\xi']\right\rangle\right)^*$ between the extremal frequencies $2\Delta_1-\xi$ and $2\Delta_2-\xi$,

$$\left\langle(\tilde{a}_{\rm out}[2\Delta_1-\xi])^\dagger\tilde{a}_{\rm out}[2\Delta_2-\xi']\right\rangle = \frac{\sin 2\theta}{2}e^{i(\varphi_2-\varphi_1)}\sinh^2\lambda\times\delta(\xi-\xi'), \quad (5)$$

which can be regarded as a coherence between the extremal, mediated by the middle vacuum

fluctuation. Owing to this vacuum-induced coherence [21–23], we obtain for the bright and dark modes

$$\left\langle (\tilde{b}_{\rm out}[\xi])^\dagger \tilde{b}_{\rm out}[\xi'] \right\rangle = \sinh^2\lambda \times \delta(\xi-\xi'), \quad (6)$$

$$\left\langle \tilde{a}_{\rm out}[\xi] \tilde{b}_{\rm out}[\xi'] \right\rangle = \frac{1}{2}\sinh 2\lambda \times \delta(\xi-\xi'), \quad (7)$$

$$\left\langle \tilde{a}_{\rm out}[\xi] \tilde{d}_{\rm out}[\xi'] \right\rangle = \left\langle \tilde{b}_{\rm out}[\xi] \tilde{d}_{\rm out}[\xi'] \right\rangle = 0, \quad (8)$$

$$\left\langle (\tilde{d}_{\rm out}[\xi])^\dagger \tilde{d}_{\rm out}[\xi'] \right\rangle = 0. \quad (9)$$

The disappearance of power in the dark mode is a particular manifestation of coherence which has been employed for many applications, such as quantum memory and STIRAP in superconducting qubit systems [24,25]. In the usual type of dark state, the destructive interference is produced at the same frequency, for example, on a quantum state of a qubit or of a mode of a field. Here, the two modes at $2\Delta_1 - \xi$ and $2\Delta_2 - \xi$ are separated in frequency and do not overlap [26]. The destructive interference effect is created by the vacuum fluctuations at ξ which trigger two correlated two-photon parametric downconversion processes in the pumps. These correlations are also reflected in the structure of the output state of the resonator $|{\rm vac}\rangle_{\rm out}$ which fulfills $\tilde{a}_{\rm out}|{\rm vac}\rangle_{\rm out} = 0$. For the truncated form of Eq. (2), the output state is a two-mode squeezed state in terms of the operators $\tilde{a}[\xi]$ and $\tilde{b}[\xi]$, $|{\rm vac}\rangle_{\rm out} = S^\dagger|{\rm vac}\rangle_{\rm in}$, where $S = \exp\left[\lambda \tilde{a}_{\rm in}\tilde{b}_{\rm in} - h.c.\right]$.

As for standard quantum interference, the lack of path information [27,28] is critical for the interference between extremal frequencies. Here, instead of which-path information in space, we deal with absence of **which-color information** [15,16] : for a real photon at frequency ξ, there is no way of knowing from which of the two spontaneous parametric downconversion processes occurring in either of the pumps, it came from.

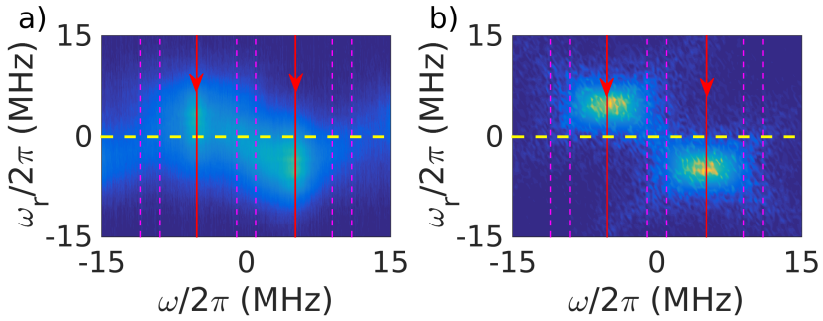

Figure 2: Measured noise power spectra corresponding to the correlator $\left\langle (\tilde{a}_{\mathrm{out}}[\xi])^{\dagger}\tilde{a}_{\mathrm{out}}[\xi]\right\rangle$ for fixed pump frequencies $\omega_1/4\pi = 4.995$ GHz, $\omega_2/4\pi = 5.005$ GHz at different values of the resonance frequency $\omega_{\mathrm{r}}/2\pi$ and measurement frequency $\omega/2\pi$ relative to $(\omega_1+\omega_2)/8\pi = 5$ GHz. a) Spectra for a pump power corresponding to average cavity occupation number of approximately 20 photons. The dashed magenta lines indicate the measurement bands within which the correlation data were collected. The red lines indicate the locations of the half of the pump frequencies ω_1 and ω_2. The dashed yellow line indicates the symmetry point which was used for measuring the data depicted in Fig. 3. b) Noise power as predicted by Eq. (2) including only first-order reflections with the parameters corresponding to a).

1 Results

To test the above predictions, we pumped our sample using two phase-locked microwave generators at frequencies 9.99 and 10.01 GHz. The output field $\tilde{a}_{\rm out}$ from the resonator is amplified yielding a signal that is next downconverted and digitized. The Fourier-transformed amplified field is measured in a bandwidth around the three frequencies of interest. The resulting fields will be denoted by $\tilde{a}_0$, $\tilde{a}_1$, $\tilde{a}_2$, corresponding to the output fields $\tilde{a}_{\rm out}[\xi]$, $\tilde{a}_{\rm out}[2\Delta_1 - \xi]$, and $\tilde{a}_{\rm out}[2\Delta_2 - \xi]$ respectively. Upon substraction of the added noise of the amplifiers, the correlations between the amplified fields provide a direct measurement of the corresponding correlations of the resonator output field [7,30] (see also Methods), up to a proportionality factor. The measured noise power data can be reproduced by simulations using the theoretical results presented earlier. The data are presented in Fig. 2 a), while the corresponding numerical result from Eq. 2 is presented in Fig. 2 b). For symmetry reasons, we chose to analyze correlations when the microwave resonance lies at half of the average of the two pump frequencies, that is $\Delta_1 \approx -\Delta_2$, in which case the tripartite correlations are strongest.

Fig. 3 displays the most relevant correlators determined as a function of the number of photons in the resonator. All these correlators can be calculated from the measured field quadratures of the output field. We find that the behavior of these correlators agrees well with the theory - squeezing correlations are seen between neighboring frequencies and vacuum-induced coherence correlations between the extremal ones. Indeed, the correlators grow nearly exponentially with pumping power, as predicted by theory. Furthermore, the ratio between various correlators is close to the expectations obtained from Eq. 2, with only the first-order pump reflections included.

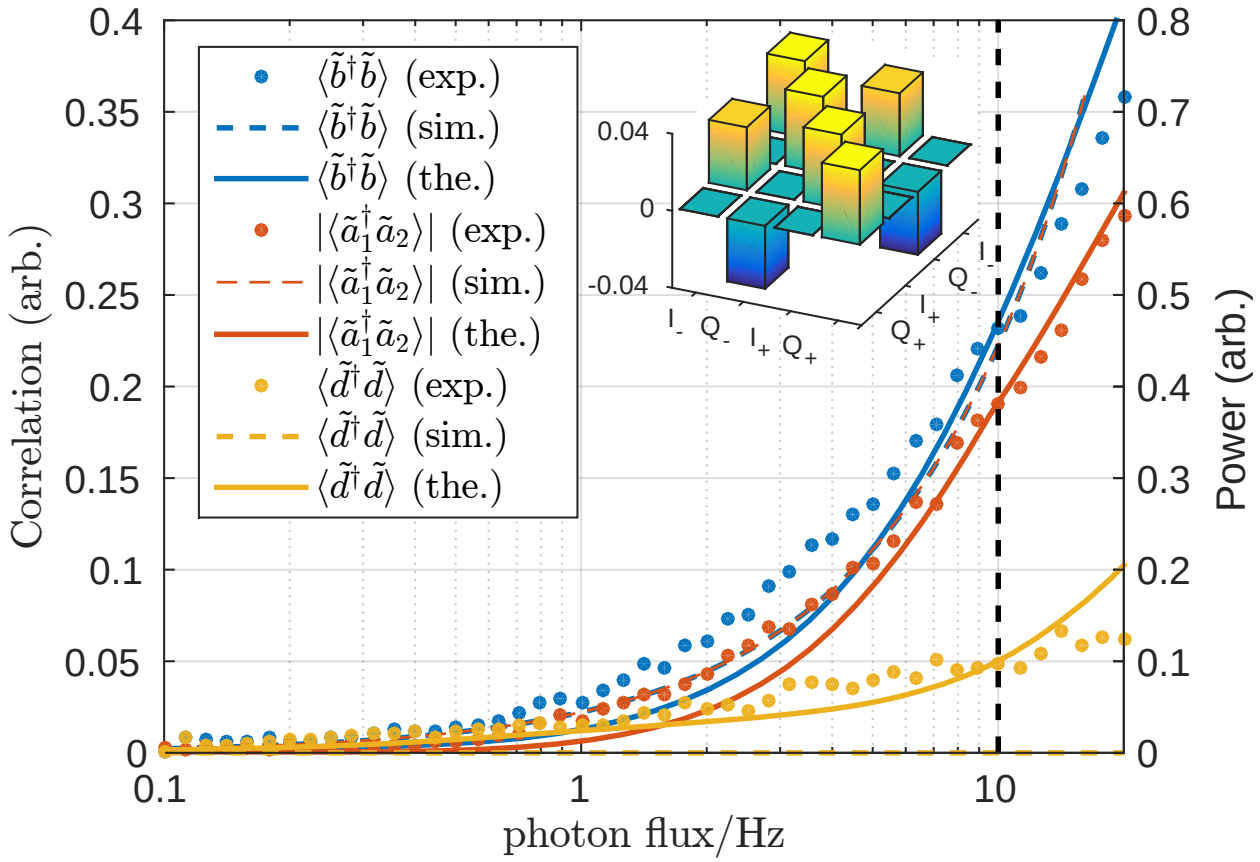

Figure 3: Measured correlators (specified in the inset label) vs. photon flux/Hz from the cavity. The symbols refer to measured data, while the curves are predictions from theory (dashed) and simulations (solid). Our simulation reproduces also the residual population in the dark mode. The 3-D histogram represents the measured covariance matrix corresponding to the fields $\tilde{a}_0$ and $\tilde{a}_1$, where the two-mode quadratures are defined as $I_0 = \frac{1}{2}(\tilde{a}_0 + \tilde{a}_0^\dagger)$, $Q_0 = \frac{1}{2i}(\tilde{a}_0 - \tilde{a}_0^\dagger)$, $I_1 = \frac{1}{2}(\tilde{a}_1 + \tilde{a}_1^\dagger)$ and $Q_1 = \frac{1}{2i}(\tilde{a}_1 - \tilde{a}_1^\dagger)$, demonstrating two-mode squeezing correlations across the first pump.

From Fig. 3 we note that the coherence is preserved also in the limit of small number of photons. This shows that our result is fundamentally different from e.g. tripartite slit-interferometer schemes [29], where the coherence between two modes is obtained only in the limit of a large number of photons in the pump mode.

The phase-dependent interplay between the bright and dark modes is presented in Fig. 4a). By adjusting the phase difference of the pumps, the measured correlator power will shift from $\langle \tilde{b}^\dagger \tilde{b} \rangle$ to $\langle \tilde{d}^\dagger \tilde{d} \rangle$ as seen in Fig. 4a along the φ_{12} axis. The division of power between the dark and bright modes depends also on the asymmetry of the two pumps, *i.e.* the parameter θ. Only if θ is correctly known, in the symmetric case $\theta = \pi/4$, the dark mode is decoupled and the correlator $\langle \tilde{d}^\dagger \tilde{d} \rangle$ becomes small. Under all parameter selections, however, the bright and dark modes remain orthogonal and $\langle \tilde{b}^\dagger \tilde{b} \rangle > \simeq 0$. Fig. 4b illustrates the change in the argument of the correlator when the phase of one pump is varied relative to the other one. We note that the possibility of applying phase shifts on the modes by the rotation of the pump phases is a key operation in continuous-variable quantum computing[13].

The creation of vacuum-induced coherence was investigated in pulsed pump tone experiments, in which the overlap of the pump signals was varied as illustrated in Fig. 5. We observe that the coherence $|\langle \tilde{a}_1^\dagger \tilde{a}_2 \rangle|$ is reduced proportionally to the decrease of pulse overlap, while the squeezings $|\langle \tilde{a}_1 \tilde{a}_0 \rangle|$ and $|\langle \tilde{a}_0 \tilde{a}_2 \rangle|$ remain. In addition, the behavior of squeezing correlations in $\langle \tilde{b}^\dagger \tilde{b} \rangle$ is indicated in Fig. 5. This demonstrates that the generation of the coherence needs overlapping pump signals, during which the which-color information is not available. When the pump pulses are separated in

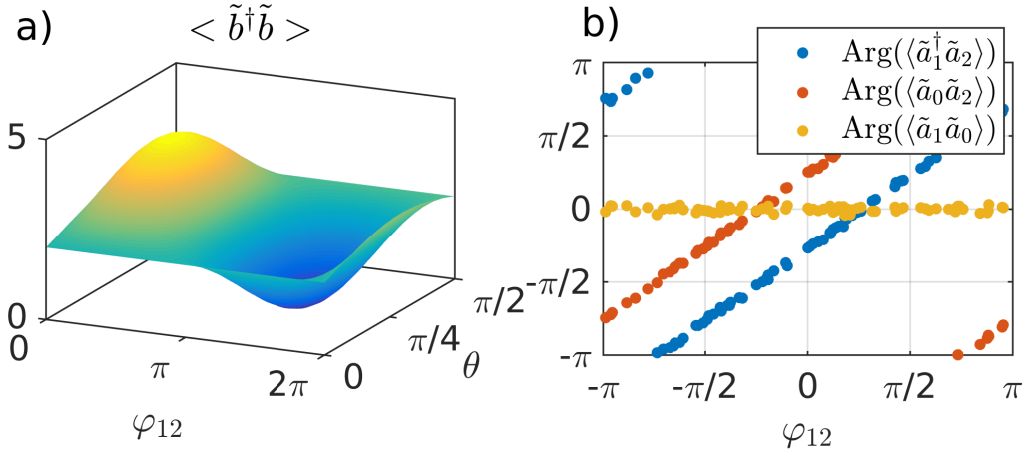

Figure 4: a) Bright/dark mode amplitude vs. phase difference between the pumps $\varphi_{12} = \varphi_1 - \varphi_2$ and pump amplitude asymmetry parameter θ (symmetric pumps have $\theta = \pi/4$). The maximum value corresponds to the bright mode amplitude while the minimum refers to the dark mode. b) Measured argument of the complex quadrature correlations vs. φ_{12}, where φ_2 is varied and $\theta \approx \pi/4$.

time, the information about which pump has generated the photons becomes accessible in principle, and the coherence is suppressed.

2 Discussions and conclusions

Our work on tripartite microwave correlations can be extended towards multipartite entangled states[31], which would yield a platform for universal quantum computation using continuous variables, a recently proposed in Ref. [14]. For example, the creation of cluster states in microwave cavities would be an important step towards realising a superconducting one-way computer. Such multipartite entangled states require pulsed microwave pumping for entangling different frequencies, a scheme that has been shown to be a fully functioning concept in our work.

We thank K. Mølmer, Sir P. Knight, and Y. Makhlin for discussions and M. Kiviranta and L. Grönberg for contributions in fabrication. This work used the cryogenic facilities of the Low Temperature Laboratory infrastructure at Aalto University. We acknowledge financial support from FQXi, the Academy of Finland project 263457, the Center of Excellence "Low Temperature Quantum Phenomena and Devices" (project 250280) and the FP7 iQuOEMS project 323924.

Author Contributions

P.L. and J.H. designed the sample. P.L. and P.H. were responsible for the experimental setup. P.L. performed the experiment and analyzed the data. G.S.P. developed the theoretical model. P.L., P.H., and G.S.P wrote the paper, and the results were discussed with all authors.

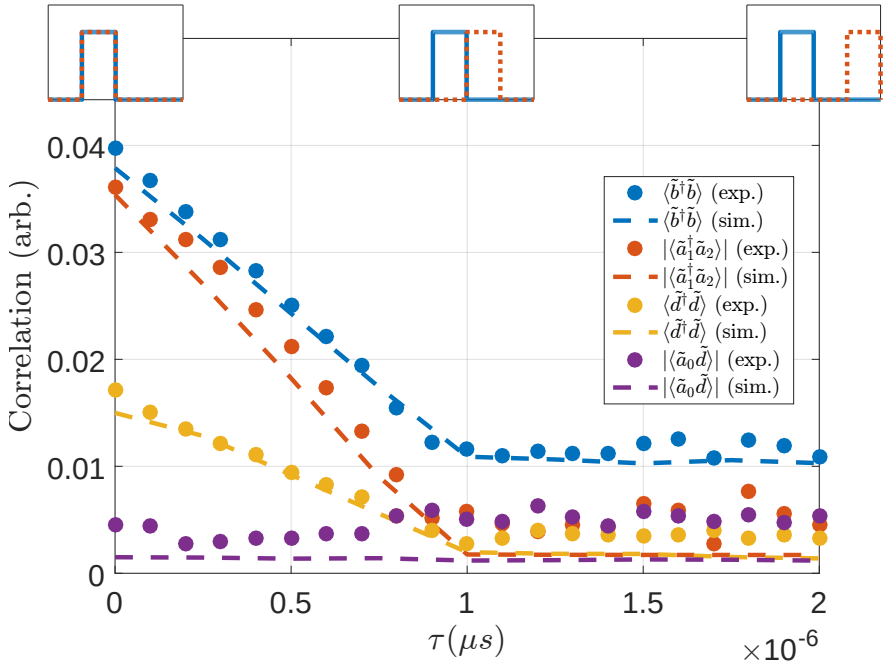

Figure 5: Decrease of vacuum-induced coherence $|\langle \tilde{a}_1^\dagger \tilde{a}_2 \rangle|$ when the overlap time τ of the parametric pumps is varied. The coherence decreases linearly (see Supplementary information) as the pumps become non-overlapping. The pulse lengths for both pump tones were set to $T_1 = T_2 = 1\mu$s, corresponding to the -3 dB bandwidth of the resonator. Other correlators specified in the label inset are also depicted. Dashed lines are from simulation and dots are from experiment. The appearance of a nonzero plateau for $\langle \tilde{b}^\dagger \tilde{b} \rangle$ with nonoverlapping pulses is due to the dynamical Casimir effect in each of the pumps separately.

Additional information

Supplementary Information accompanies this paper. **Competing financial interests:** The authors declare no competing financial interests.

3 Methods

Numerical evaluation of correlators

The numerically simulated results presented in Fig. 2 and Fig. 3 were obtained using Gaussian (white) noise to represent the effect of the vacuum as input. Additionally, higher order reflections were included in Fig. 3 by solving the Heisenberg-Langevin equation (HLE) in the rotating-wave approximation (RWA) $\dot{\tilde{a}} = \sum_{p=1,2} \alpha_p e^{-2i\Delta_p} \tilde{a}^\dagger - \frac{\kappa}{2}\tilde{a} - \sqrt{\kappa}\tilde{a}_{\rm in}$. The presumption of white noise is accurate for narrow bandwidths where the spectrum of quantum noise is approximately uniform. In this way, higher-order reflections are included automatically in the results.

As seen from Fig. 3, the simple tripartite analytical solution of Eq. (2), leading to correlators listed in Eqs. (5-9), agrees quite well with the results, except for the dark mode correlator $\langle \tilde{d}^\dagger \tilde{d} \rangle$. The disagreement can be traced to the assumption $\xi \ll \Delta_1, \Delta_2$, but the numerical simulations are not limited by this approximation.

Homodyne detection of correlations

The output field of the resonator propagates through circulators and is amplified by a cryogenic low noise HEMT amplifier and by room-temperature microwave amplifiers. The qudratures are measured by standard homodyne methods, i.e. captured using Anritsu MS2830A signal analyzer. Approximately 20 GB of data per sweep were collected and transferred to PC for later analysis. The single bins of the Fourier transformed data represent a bandwidth of 50 Hz and, therefore, spectral

leakage due to used rectangular windowing is insignificant.

From the quadratures we can construct the complex field amplitudes, calculate their Fourier components around the central and extremal frequencies, in a bandwidth BW. We can write

$$\tilde{a}_0 = \int_{-\infty}^{\infty} d\varsigma f_{(BW)}[\xi;\varsigma]\tilde{a}_{\rm out}[\varsigma], \tag{10}$$

$$\tilde{a}_{1,2} = \int_{-\infty}^{\infty} d\varsigma f_{(BW)}[2\Delta_{1,2}-\xi;\varsigma]\tilde{a}_{\rm out}[\varsigma], \tag{11}$$

where $f_{(BW)}[\xi;\varsigma]$ is a digital filtering function of width BW centered at the frequency ξ. Choosing $\int_{-\infty}^{\infty} d\varsigma |f_{(BW)}[\xi;\varsigma]|^2 = 1$ ensures that $[\tilde{a}_0, \tilde{a}_0^\dagger] = 1$, $[\tilde{a}_1, \tilde{a}_1^\dagger] = 1$, $[\tilde{a}_2, \tilde{a}_2^\dagger] = 1$. A simple choice is $f_{(BW)}[\xi;\varsigma] = 1/\sqrt{BW}$ if ς is in the interval $(\xi - BW/2, \xi + BW/2)$, and 0 otherwise.

Because the added noise of the measurement chain is contained in $\tilde{a}_{\rm out}$ and uncorrelated, its contribution will vanish when calculating the correlations of $\tilde{a}_{0,1,2}$ and in the case of autocorrelation, it can be subtracted as a known constant. We can obtain then directly from Eqs. (10) and (11) all the measured correlations, for example $\langle \tilde{a}_0 \tilde{a}_1 \rangle = \frac{1}{2}\cos\theta \exp(i\varphi_1)\sinh(2\lambda)$, etc.

Pulsed parametric pumping

In pulsed measurements, the pumping tones (corresponding to 50 quanta occupation of the resonator in continuous operation) were modulated using a pair of mixers (Marki M10220LA), driven by digital delay generators from Stanford Research System (DG535). The system provides an ON/OFF ratio of 1:100 and a rise time of 10 ns. The repetition rate was set to 250 kHz, which resulted in signals of 30% when compared to continuous measurements. With a pulse width of $T_1 = T_2 = 1$ μs, the repetition rate corresponds to a duty cycle of 1:3. This signal sets the

background level (duty cycle $\times$ continuous DCE) in the pulsed experiments of the correlation function $\langle \tilde{b}^\dagger \tilde{b} \rangle$. The same method of simulating the Heisenberg-Langevin equations in time domain was employed to calculate numerically the response for pulsed pump tones.

1. Clerk, A. A., Devoret, M. H., Girvin, S. M., Marquardt, F. & Schoelkopf, R. J. Introduction to quantum noise, measurement, and amplification. *Rev. Mod. Phys.* **82**, 1155–1208 (2010). URL http://link.aps.org/doi/10.1103/RevModPhys.82.1155.

2. You, J. Q. & Nori, F. Atomic physics and quantum optics using superconducting circuits. *Nature* **474**, 589–597 (2011). URL http://dx.doi.org/10.1038/nature10122. arXiv:1202.1923v1.

3. Nation, P. D., Johansson, J. R., Blencowe, M. P., Nori, Franco Colloquium: Stimulating uncertainty: Amplifying the quantum vacuum with superconducting circuits. *Rev. Mod. Phys.* **84**, 0034–6861 (2012). URL http://link.aps.org/doi/10.1103/RevModPhys.84.1.

4. Yurke, B. *et al.* Observation of 4.2-K equilibrium-noise squeezing via a Josephson-parametric amplifier. *Phys. Rev. Lett.* **60**, 764–767 (1988). URL http://link.aps.org/doi/10.1103/PhysRevLett.60.764.

5. Castellanos-Beltran, M. A., Irwin, K. D., Hilton, G. C., Vale, L. R. & Lehnert, K. W. Amplification and squeezing of quantum noise with a tunable Josephson metamaterial. *Nat. Phys.* **4**, 929–931 (2008). URL http://dx.doi.org/10.1038/nphys1090.

6. Mallet, F. *et al.* Quantum State Tomography of an Itinerant Squeezed Microwave Field. *Phys. Rev. Lett.* **106**, 220502 (2011). URL http://link.aps.org/doi/10.1103/PhysRevLett.106.220502.

7. Eichler, C. *et al.* Observation of Two-Mode Squeezing in the Microwave Frequency Domain. *Phys. Rev. Lett.* **107**, 113601 (2011). URL http://link.aps.org/doi/10.1103/PhysRevLett.107.113601.

8. Wilson, C. M. *et al.* Observation of the dynamical Casimir effect in a superconducting circuit. *Nature* **479**, 376–9 (2011). URL http://dx.doi.org/10.1038/nature10561.

9. Lähteenmäki, P., Paraoanu, G. S., Hassel, J. & Hakonen, P. J. Dynamical Casimir effect in a Josephson metamaterial. *Proc. Natl. Acad. Sci.* **110**, 4234–4238 (2013). URL http://www.pnas.org/cgi/doi/10.1073/pnas.1212705110. 1111.5608.

10. Menzel, E. P. *et al.* Path Entanglement of Continuous-Variable Quantum Microwaves. *Phys. Rev. Lett.* **109**, 250502 (2012). URL http://link.aps.org/doi/10.1103/PhysRevLett.109.250502.

11. Yuen, H. P. Two-photon coherent states of the radiation field. *Phys. Rev. A* **13**, 2226–2243 (1976).

12. Caves, C. M. & Schumaker, B. L. New formalism for 2-photon quantum optics. 1. Quadrature phases and squeezed states. *Phys. Rev. A* **31**, 3068–3092 (1985). URL http://dx.doi.org/10.1103/PhysRevA.31.3068.

13. Braunstein, S. L. & van Loock, P. Quantum information with continuous variables. *Rev. Mod. Phys.* **77**, 513–577 (2005). URL http://link.aps.org/doi/10.1103/RevModPhys.77.513. 0410100.

14. Bruschi, D., *et al.* Towards universal quantum computation through relativistic motion. *arXiv 1311.5619v2* 22 (2013). URL http://arxiv.org/abs/1311.5619. 1311.5619.

15. Zou, X. Y., Wang, L. J. & Mandel, L. Induced coherence and indistinguishability in optical interference. *Phys. Rev. Lett.* **67**, 318–321 (1991). URL http://link.aps.org/doi/10.1103/PhysRevLett.67.318.

16. Kim, Y.-H., Yu, R., Kulik, S. P., Shih, Y. & Scully, M. O. Delayed Choice Quantum Eraser. *Phys. Rev. Lett.* **84**, 1–5 (2000). URL http://link.aps.org/doi/10.1103/PhysRevLett.84.1.

17. Kelly, W. R. *et al.* Direct observation of coherent population trapping in a superconducting artificial atom. *Phys. Rev. Lett.* **104**, 1–4 (2010). 0912.3291.

18. Marquardt, F., Chen, J. P., Clerk, A. A. & Girvin, S. M. Quantum Theory of Cavity-Assisted Sideband Cooling of Mechanical Motion. *Phys. Rev. Lett.* **99**, 093902 (2007). URL http://link.aps.org/doi/10.1103/PhysRevLett.99.093902.

19. Zakka-Bajjani, E. *et al.* Quantum superposition of a single microwave photon in two different colour states. *Nat. Phys.* **7**, 599–603 (2011). URL http://dx.doi.org/10.1038/nphys2035.

20. Kiviranta, M., Brandel, O., Grönberg, L., Kunert, J., Linzen, S., Beev, N., Prunnila, M. Multilayer fabrication process for josephson junction circuits cross-compatible over two foundries. *Supercond. Sci. Technol.* submitted (2015).

21. Arimondo, E. & Wolf, E. Coherent population trapping in laser spectroscopy. *Prog. Opt.* **35**, 257–354 (1996). URL https://jila.colorado.edu/publications/coherent-population-trapping-laser-spectroscopy.

22. Tanji-Suzuki, H., Chen, W., Landig, R., Simon, J. & Vuletic, V. Vacuum-Induced Transparency. *Science* **333**, 1266–1269 (2011). URL http://www.sciencemag.org/cgi/doi/10.1126/science.1208066.

23. Agarwal, G. S. *Quantum Optics*. Quantum Optics (Cambridge University Press, 2012). URL https://books.google.fi/books?id=7KKw_XIYaioC.

24. Zhu, X. *et al.* Observation of dark states in a superconductor diamond quantum hybrid system. *Nat. Commun.* **5**, 3424 (2014). URL http://www.nature.com/ncomms/2014/140408/ncomms4524/full/ncomms4524.html.

25. Kumar, K. S., Vepsäläinen, A., Danilin, S. & Paraoanu, G. S. Stimulated Raman adiabatic passage in a three-level superconducting circuit. **arXiv 1508.02981v1** 1–10 (2015). URL http://arxiv.org/abs/1508.02981. 1508.02981.

26. Ramelow, S., Ratschbacher, L., Fedrizzi, A., Langford, N. K. & Zeilinger, A. Discrete tunable color entanglement. *Phys. Rev. Lett.* **103**, 2–5 (2009).

27. Lemos, G. B. *et al.* Quantum imaging with undetected photons. *Nature* **512**, 409–412 (2014). URL http://dx.doi.org/10.1038/nature13586.

28. Ma, X.-S., Kofler, J. & Zeilinger, A. Delayed-choice gedanken experiments and their realizations. **arXiv:1407** (2014).

29. Bertet, P., *et al.* A complementarity experiment with an interferometer at the quantum-classical boundary, *Nature* **411**, 166-170 (2001).

30. da Silva, M. P., Bozyigit, D., Wallraff, A. & Blais, A. Schemes for the observation of photon correlation functions in circuit QED with linear detectors. *Phys. Rev. A* **82**, 043804 (2010). URL http://link.aps.org/doi/10.1103/PhysRevA.82.043804.

31. Chen, M., Menicucci, N. C. & Pfister, O. Experimental Realization of Multipartite Entanglement of 60 Modes of a Quantum Optical Frequency Comb. *Phys. Rev. Lett.* **112**, 120505 (2014). URL http://link.aps.org/doi/10.1103/PhysRevLett.112.120505.